

TIPE3 Is the Transfer Protein of Lipid Second Messengers that Promote Cancer

Svetlana A. Fayngerts,¹ Jianping Wu,² Camilla L. Oxley,³ Xianglan Liu,⁴ Anastassios Vourekas,¹ Terry Cathopoulos,¹ Zhaojun Wang,¹ Jian Cui,⁴ Suxia Liu,⁴ Honghong Sun,¹ Mark A. Lemmon,³ Lining Zhang,⁴ Yigong Shi,^{2,*} and Youhai H. Chen^{1,*}

¹Department of Pathology and Laboratory Medicine, Perelman School of Medicine, University of Pennsylvania, Philadelphia, PA 19104, USA

²School of Life Sciences, Tsinghua University, Beijing 100084, China

³Department of Biochemistry and Biophysics, Perelman School of Medicine, University of Pennsylvania, Philadelphia, PA 19104, USA

⁴Institute of Immunology, School of Medicine, Shandong University, Jinan, Shandong 250012, China

*Correspondence: ygshi@tsinghua.edu.cn (Y.S.), yhc@mail.med.upenn.edu (Y.H.C.)

<http://dx.doi.org/10.1016/j.ccr.2014.07.025>

SUMMARY

More than half of human cancers have aberrantly upregulated phosphoinositide signals; yet how phospholipid signals are controlled during tumorigenesis is not fully understood. We report here that TIPE3 (TNFAIP8L3) is the transfer protein of phosphoinositide second messengers that promote cancer. High-resolution crystal structure of TIPE3 shows a large hydrophobic cavity that is occupied by a phospholipid-like molecule. TIPE3 preferentially captures and shuttles two lipid second messengers, i.e., phosphatidylinositol 4,5-bisphosphate and phosphatidylinositol 3,4,5-trisphosphate, and increases their levels in the plasma membrane. Notably, human cancers have markedly upregulated TIPE3 expression. Knocking out TIPE3 diminishes tumorigenesis, whereas enforced TIPE3 expression enhances it in vivo. Thus, the function and metabolism of phosphoinositide second messengers are controlled by a specific transfer protein during tumorigenesis.

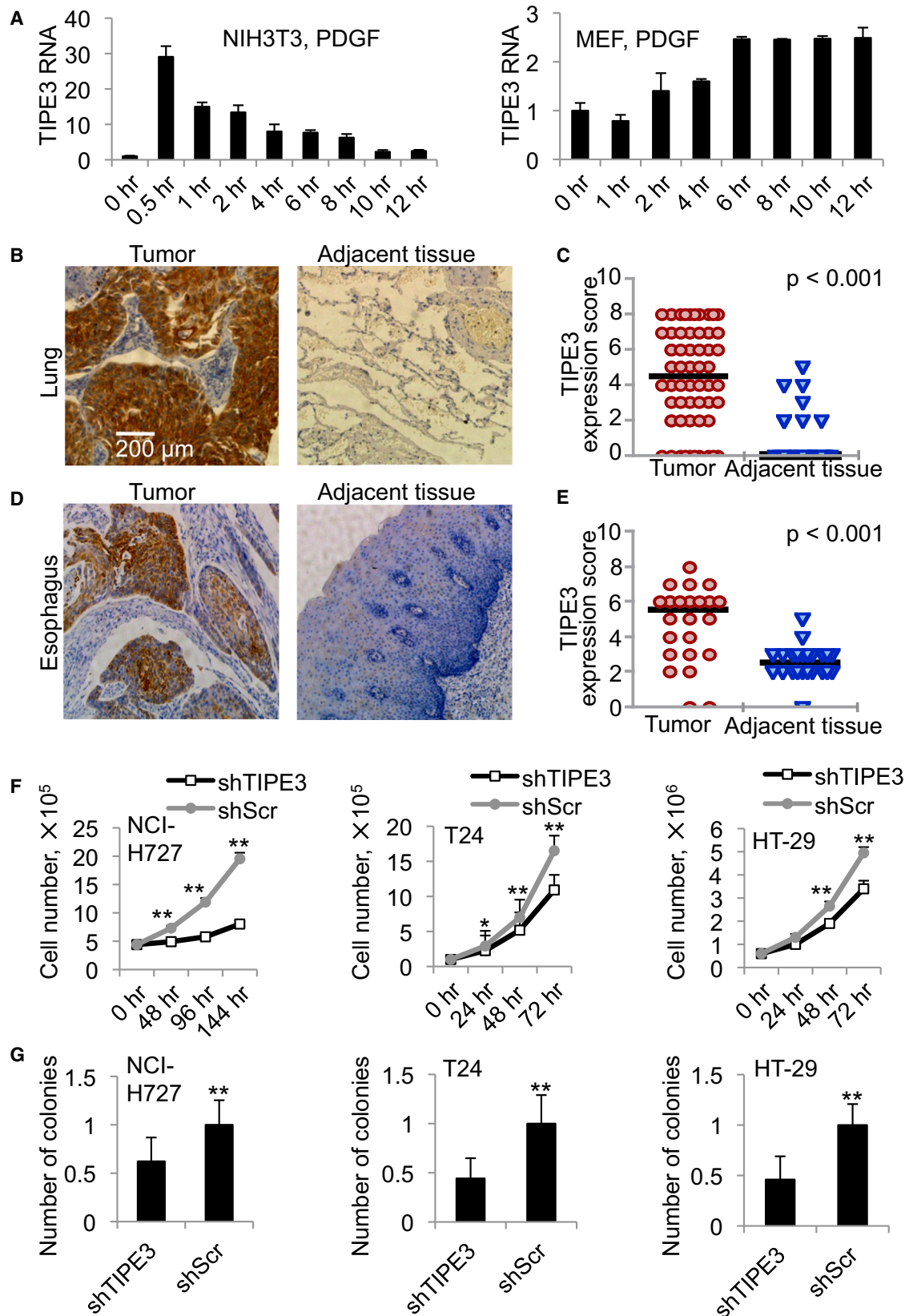
INTRODUCTION

Tumorigenesis is a multistep process orchestrated by several classes of molecules that control cell death and/or growth. The TNFAIP8 (tumor necrosis factor- α -induced protein 8, or TIPE) family of proteins has been recently described as regulators of tumorigenesis and inflammation (Kumar et al., 2004; Sun et al., 2008). TNFAIP8 promotes tumor metastasis and is a risk factor for non-Hodgkin's lymphoma in humans and for bacterial infection in mice (Ahn et al., 2010; Zhang et al., 2012). Similarly, TIPE2 (TNFAIP8L2) regulates both carcinogenesis and inflammation, and its germline deletion leads to fatal inflammatory diseases (Gus-Brautbar et al., 2012; Sun et al., 2008; Wang et al., 2012). TIPE1 has been reported to regulate cell death (Hitomi et al., 2008), whereas the role of TIPE3 has not yet been described. How TNFAIP8 family regulates tumorigenesis is largely unknown.

Phosphoinositides constitute approximately 1% of lipids in the eukaryotic plasma membrane, but they play a major role as signaling molecules in both normal and tumor cells. There are seven phosphoinositides, which are generated by phosphorylation of the inositol ring of phosphatidylinositol (PtdIns) on the third, fourth, and/or fifth hydroxyl groups (Fruman et al., 1998). PtdIns 4,5-bisphosphate (PtdIns(4,5) P_2) plays key signaling roles (Kwiatkowska and Sobota, 1999; McLaughlin et al., 2002). It is the precursor of at least three second messengers: inositol 1,4,5-trisphosphate (Ins(1,4,5) P_3) and diacylglycerol generated through hydrolysis by phospholipase C (PLC) isoforms; and PtdIns(3,4,5) P_3 generated through phosphorylation by phosphoinositide-3 kinases (PI3Ks). More than half of human cancers have aberrantly upregulated PtdIns(3,4,5) P_3 or PtdIns(4,5) P_2 signals. While somatic mutations of PTEN, Ras, and the α catalytic subunit of PI3K (PIK3CA) account for many cases of the phosphoinositide signaling upregulation, other mechanisms of the

Significance

More than half of human cancers have aberrantly upregulated phosphoinositide signals; yet how lipid signals are controlled in cancer cells is not fully understood. The TNFAIP8 family of proteins has been recently described as a risk factor for human cancer, although its mechanisms of action are largely unknown. We report here that TIPE3 (TNFAIP8L3) is the transfer protein of two lipid second messengers, PtdIns(4,5) P_2 and PtdIns(3,4,5) P_3 , and is hijacked by cancer cells to cause malignant transformation. This finding explains why normal cells can control their phospholipid signals but cancer cells cannot, a phenomenon widely recognized but poorly understood. Therefore, TIPE3 may represent a therapeutic target for treating malignant diseases.



(legend on next page)

dysregulation are being discovered as well (Vivanco and Sawyers, 2002; Yuan and Cantley, 2008). In this report, we describe a mammalian transfer protein for PtdIns(4,5) P_2 and PtdIns(3,4,5) P_3 and examine its role in phosphoinositide signaling.

RESULTS

TIPE3 Is Markedly Upregulated in Four Types of Human Cancers and in Cells Treated with Growth Factors

TIPE3 is expressed in a wide range of organs, but its expression levels vary greatly (Figure S1A available online). High levels of TIPE3 messenger RNA (mRNA) were detected in murine uterus and developing embryos, whereas little or no TIPE3 was detected in lymphoid organs. Moderate expression of TIPE3 was observed in many organs, including intestine, lung, brain, bladder, and colon (Figure S1A). Similarly, murine and human cell lines have varying levels of TIPE3 expression (Figures S1B and S1C). It is interesting that, when treated with platelet-derived growth factor (PDGF), serum-starved NIH 3T3 cells and primary murine embryonic fibroblasts (MEFs) both markedly upregulated TIPE3 expression in a time-dependent manner (Figure 1A).

To determine TIPE3 expression in human tumors, we studied, by immunohistochemistry, tumor samples from 60 lung cancer patients and 24 esophageal cancer patients. Marked upregulation of TIPE3 protein was observed in the majority of tumor sections compared with adjacent nontumor sections from the same patients (Figures 1B–1E; Figures S1D and S1E). Additionally, we also detected significant TIPE3 upregulation in human cervical cancer (70 patients) and colonadenocarcinoma (82 patients) (data not shown). These results indicate that, similar to other TIPE proteins, TIPE3 may be involved in tumorigenesis.

Overexpressing TIPE3 Promotes Tumorigenesis, whereas Knocking out TIPE3 Inhibits It

To explore the potential role of TIPE3 in tumorigenesis, we used knockdown, knockout, and overexpression approaches. Transfection with a short hairpin RNA (shRNA) that targets TIPE3 (shTIPE3) significantly reduced TIPE3 expression in three human cancer cell lines: NCI-H727 lung carcinoma cells (with KRasV12 and PIK3CAE545 mutations), T24 bladder carcinoma cells (with HRasV12 mutation), and HT-29 colorectal adenocarcinoma cells (with PIK3CAT449 and BRAFV600E mutations) (Figures S1F and S1G). This was associated with significant reduction in total cell numbers (Figure 1F) and compromised ability of the cells to form colonies in soft agar (Figure 1G). Conversely, when overexpressed, TIPE3 significantly increased the numbers of 293T cells

with HRasV12 or PIK3CAE545 mutation (Figure S2A) and of HRasV12-transformed NIH 3T3 cells (NIH 3T3-HRasV12) (Figure 2A). TIPE3 overexpression also increased the size of the colonies formed in soft agar (Figures 2B and S2B) and accelerated cell cycle progression as evidenced by a reduced population of G0/G1 cells and increased S/G2/M cells (Figure 2C). These results indicate that TIPE3 promotes tumor cell growth in vitro.

To examine the effect of TIPE3 on tumorigenesis in vivo, we first injected NIH 3T3-HRasV12 cells with or without TIPE3 overexpression into nude mice (*nu/nu*). Strikingly, both tumor onset and tumor growth were significantly accelerated in the TIPE3 group (Figure 2D). By day 10 following tumor cell injection, tumors of the TIPE3 group were twice as large as those of the control group ($p < 0.05$, $n = 14$) (Figures 2E and S2C). The difference in tumor size was most likely due to enhanced proliferation of the TIPE3-overexpressing cells because increased bromodeoxyuridine (BrdU) incorporation was observed in tumor sections of the TIPE3 group (Figures 2F and S2D). Cell death, as determined by cleaved (active) caspase-3 staining, may also play a role because 0.86% cells in TIPE3-transfected tumors underwent cell death compared to 1.94% cells in the control tumors (Figure S2E).

Next, we studied carcinogen-induced tumorigenesis in the recently generated *Tipe3* knockout (*Tipe3*^{-/-}) mice (Figure S2F). Under pathogen-free conditions, these mice developed normally and did not exhibit noticeable signs of spontaneous diseases during the first 3 months of their lives (data not shown). However, following subcutaneous injection with the carcinogen 3-methylcholanthrene, *Tipe3*^{-/-} mice exhibited a markedly delayed skin tumor onset and reduced tumor size in comparison with wild-type (WT) mice (Figures 2G and 2H). As expected, *Tipe3*^{-/-} fibrosarcoma cells grew much slower than WT controls in the culture (Figure 2I).

The Unique N-Terminal Region of TIPE3 Is Essential for Its Effect on Cell Growth and Survival

Unlike other members of the TNFAIP8 family that were capable of inducing cell death, TIPE3 did not reduce cell viability in the culture (Figures S2A and S2G). To the contrary, when overexpressed in NIH 3T3 cells, TIPE3 was able to increase the percentage of S phase cells, even in the absence of the oncogenic Ras (Figure 3A). Consistent with this observation, TIPE3 drives cap-dependent protein synthesis required for G1-S transition. Cotransfection of TIPE3-expressing vector and green fluorescence protein (GFP)-expressing vector that contained a cap-dependent translation initiation site significantly increased the

Figure 1. Upregulation of TIPE3 Expression Correlates with Tumorigenesis

(A) RT-PCR analyses of TIPE3 mRNA levels in the NIH 3T3 fibroblast cell line (left) and C57BL/6 MEFs (right). Cells were first serum starved for 12 hr and then stimulated with 20 (left) and 50 (right) ng/ml of PDGF for the indicated times before being collected for the RNA analyses. The expression levels of TIPE3 in NIH 3T3 (right) and MEF (left) at 0 hr were set as 1.

(B–E) TIPE3 upregulation in human cancers. Immunohistochemistry analyses of TIPE3 protein expression in tumors and their adjacent normal tissues from patients diagnosed with lung cancer (B and C) and esophageal cancer (D and E). TIPE3-positive cells are shown in brown (B and D). Quantitation of the TIPE3 expression in tumors and adjacent tissues of 60 patients with lung cancer (C) and 24 patients with esophageal cancer (E) was performed as described in Supplemental Experimental Procedures. Each data point represents a TIPE3 expression score of patients. The horizontal bars represent the medians.

(F) Cell growth analysis of human NCI-H727, T24, and HT-29 cells stably expressing either shTIPE3 or short hairpin scrambled (shScr) RNA (control) over the indicated times.

(G) Soft agar colony formation of NCI-H727, T24, and HT-29 cells expressing either shTIPE3 or shScr. Numbers of colonies formed by cells expressing shScr were set as 1.

For (A), (F), and (G), values represent means \pm SD. * $p < 0.05$; ** $p < 0.01$. The experiments were repeated at least three times with similar results. See also Figure S1.

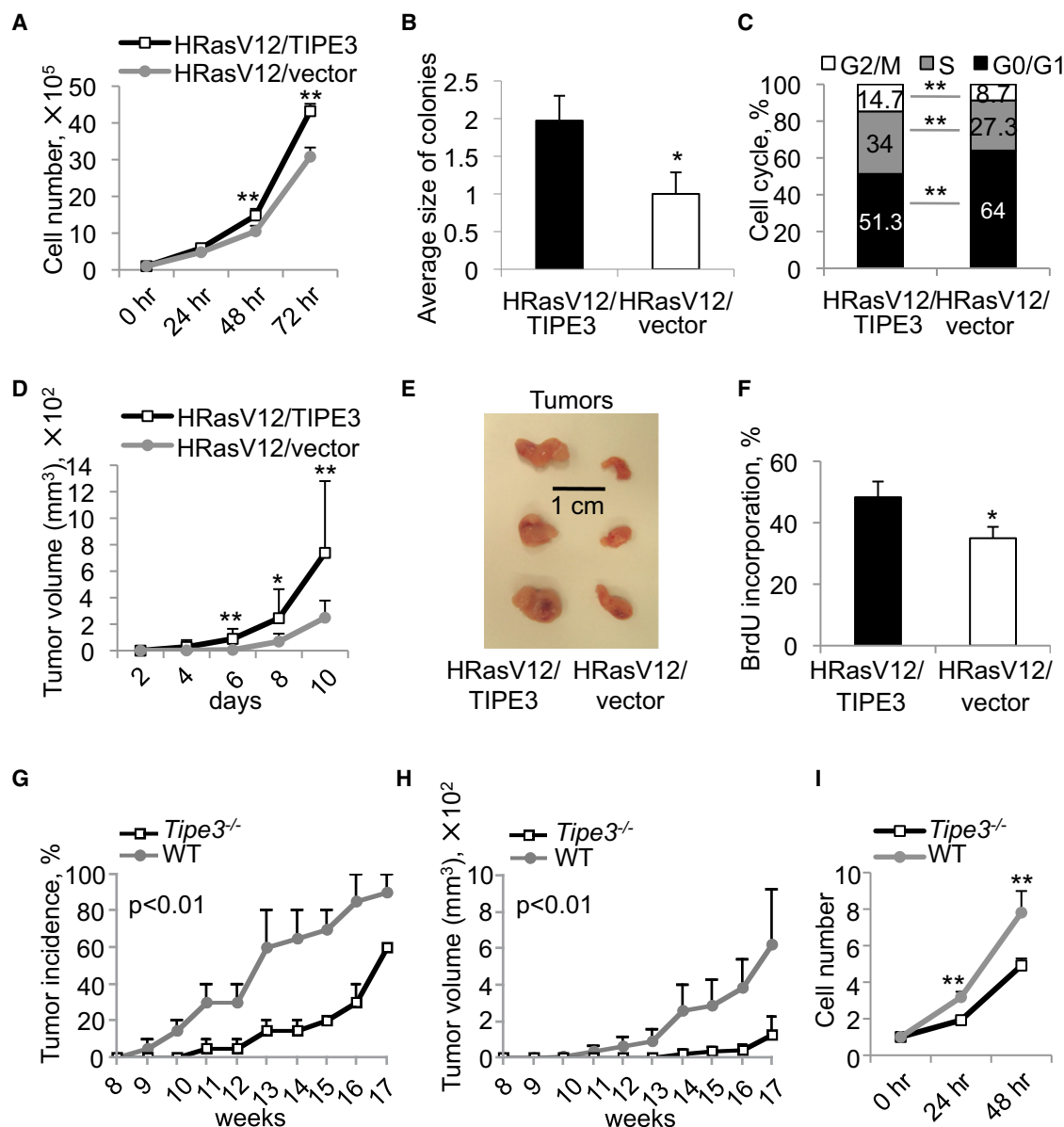


Figure 2. TIPE3 Promotes Tumorigenesis, Cell Growth, and Cell Survival In Vitro and In Vivo

(A–C) Analyses of cell growth (A), relative colony size in soft agar (B), and cell cycle progression (C) of NIH 3T3–HRasV12 cells stably transfected with either TIPE3–Flag or empty vector. For (B), number of colonies formed by NIH 3T3–HRasV12 cells transfected with empty vector was set as 1. The experiments were repeated at least three times with similar results. Values represent means \pm SD.

(D–F) TIPE3 promotes tumor growth in a murine xenograft model. Nude mice ($n = 14$) were injected subcutaneously with NIH 3T3–HRasV12 cells stably transfected with either TIPE3–Flag or empty vector. (D) Tumor volume was determined over a course of 10 days. (E) At day 10, tumors were excised and photographed. In vivo cell proliferation was analyzed by BrdU incorporation. (F) The percentages of BrdU-positive cells in tumor sections are shown. Results are representative of two independent experiments. Values represent means \pm SD.

(G–I) *Tipe3* deficiency reduces tumor growth in mice. *Tipe3*^{-/-} mice and wild-type (WT) controls ($n = 15$), 7 weeks of age, were injected subcutaneously with 3-methylcholanthrene. (G) Tumor incidence was examined for up to 17 weeks. Data are pooled from two independent experiments. (H) Tumor volume was monitored for up to 17 weeks. Results are representative of two independent experiments. Values represent means \pm SEM; the p values shown are for differences after week 11. (I) Growth of *Tipe3*^{-/-} and WT fibrosarcoma cells over the indicated times. Data are pooled from three independent *Tipe3*^{-/-} and two independent WT fibrosarcoma cell cultures established from different 3-methylcholanthrene-induced tumors. The cell numbers at 0 hr were set as 1. The experiments were repeated four times with similar results.

Values represent means \pm SD. * $p < 0.05$; ** $p < 0.01$. See also Figure S2.

expression of GFP (Figure 3B). The TIPE3 effect was less apparent in cells transfected with a GFP-expressing vector that contained an internal ribosome entry site (Figure S3A). The

effect of TIPE3 on cap-dependent GFP expression was significantly reduced by the PI3K inhibitor LY294002 and/or the MEK-ERK pathway inhibitor PD98059 (Figure S3B), indicating

that TIPE3 may play a role in the regulation of the PI3K-AKT and MEK-ERK signaling pathways.

As stated earlier, TIPE3 overexpression reduced the percentage of dying tumor cells in nude mice. In vitro, a similar effect was observed in cultured NIH 3T3 cells. TIPE3 significantly decreased serum deprivation-induced death of NIH 3T3 cells, as assessed by trypan blue staining (Figure 3C) and cleaved caspase-3 staining (Figure S3C), and the addition of the PI3K inhibitor LY294002 abolished this effect (Figures S3C and S3D).

All TIPE family proteins contain a highly conserved TIPE2 homology (TH) domain consisting of seven α helices (Figure S3E) (Zhang et al., 2009). TIPE3 has a unique N-terminal (NT) sequence of 19 amino acids, designated as the NT region here, which is not seen in other members of the TIPE family. Hypothesizing that the TIPE3 NT region is important for its unique ability to promote cell growth and survival, we investigated the effect of deleting it. A truncated TIPE3 variant lacking amino acids 2–20 (trTIPE3) not only lost the function of TIPE3 but also appeared to exert a dominant negative effect. Overexpression of trTIPE3 significantly reduced cell growth, decreased the number of S-phase cells, enhanced cell death, and reduced cap-dependent translation (Figures 3D–3I). The trTIPE3 effect on serum starvation-induced cell death was not further enhanced by LY294002, suggesting that trTIPE3 might inhibit the PI3K pathway (Figure 3F). Notably, when cotransfected into the same cells, the inhibitory effects of trTIPE3 on cell growth and death prevailed over those of WT TIPE3, indicating that trTIPE3 may function in a dominant negative fashion (Figures 3J and 3K). It is to be noted that location of the Flag-tag did not affect TIPE3 functions (Figures 3L and 3M). TIPE2, another member of the TIPE family that exhibits similar activities as trTIPE3 in cell growth and death, completely lost its function when fused to the NT region of TIPE3 (Figures 3L and 3M).

TIPE3 Promotes Activation of the PI3K-AKT and MEK-ERK Pathways

TIPE3 overexpression in NIH 3T3 cells substantially enhanced AKT phosphorylation, whereas trTIPE3 overexpression reduced it, and similar effects were seen for phosphorylation of ERK and p70S6K (Figure 4A; Figure S4A). Both AKT and ERK regulate cyclin D1 levels and thus influence cell cycle G1-S transition. Cyclin D1 levels were elevated in NIH 3T3 cells transfected with TIPE3 and decreased in cells transfected with trTIPE3 (Figures 4A and S4A). Additionally, TIPE3 enhanced HRasV12-induced phosphorylation of AKT and ERK in NIH 3T3 cells (Figures 4A and S4A).

On the other hand, TIPE3 knockdown human NCI-H727 and T24 carcinomas cells and *Tipe3* knockout murine fibrosarcoma cells showed significantly decreased phosphorylation of both AKT and ERK (Figure 4B; Figures S4B and S4C). In HT-29 cells, TIPE3 knockdown impaired AKT activation but did not affect ERK activation.

To gain more insight into TIPE3-mediated regulation of AKT and ERK activation, we treated NIH 3T3 cells with PDGF in the absence or presence of overexpressed TIPE3. PDGF markedly increased the levels of phosphorylated AKT and ERK, which were further augmented by TIPE3 (Figures 4C and 4D; Figures S4D and S4E). The PI3K inhibitor LY294002 completely blocked AKT phosphorylation, whereas rapamycin that inhibits the

mammalian target of rapamycin had no effect (Figures 4C and S4D), indicating that TIPE3 amplifies PI3K-dependent activation of AKT. However, LY294002 did not change the level of ERK phosphorylation, whereas PD98059, a MEK inhibitor, abolished ERK phosphorylation entirely, with or without TIPE3 overexpression. It is interesting that U-73122, an inhibitor of PLC, and bisindolylmaleimide I, an inhibitor of PKC, overpowered the effect of TIPE3 on ERK phosphorylation (Figures 4D and S4E).

TIPE3 Regulates Phosphoinositide Metabolism and Signaling

We observed significant increases in the total levels of PtdIns(4,5) P_2 in TIPE3-overexpressing cells using three approaches: protein-lipid overlay assay with PLC δ -Pleckstrin homology (PH) domain that specifically binds PtdIns(4,5) P_2 (Figure 4E), immunofluorescence confocal microscopy of fixed cells with anti-PtdIns(4,5) P_2 antibody (Figures S4F and S4G), and immunoblotting with an anti-PtdIns(4,5) P_2 antibody (Figure S4H). Similarly, the total pool of PtdIns(3,4,5) P_3 was also markedly increased (~4-fold) in TIPE3-overexpressing cells (Figures 4E and S4H). Consistent with these results, significant reductions in the PtdIns(4,5) P_2 and PtdIns(3,4,5) P_3 cellular levels were observed in *Tipe3* knockout murine fibrosarcoma cells as compared to WT cells (Figure S4I). The effect of overexpressed TIPE3 was dependent on the NT region since the trTIPE3 that lacks it decreased PtdIns(4,5) P_2 and PtdIns(3,4,5) P_3 levels (Figure S4J).

To visualize changes in PtdIns(4,5) P_2 and PtdIns(3,4,5) P_3 levels following stimulation of cells with PDGF, we performed confocal microscopy of fixed cells using GFP-tagged PH domains. In untreated NIH 3T3 cells, PLC δ -PH-GFP, which selectively binds PtdIns(4,5) P_2 , was localized predominantly to the plasma membrane (Figure 5A; Figure S5A). PDGF stimulation (for 5.5 min) significantly reduced membrane-bound but increased cytoplasmic PLC δ -PH-GFP signals, which is consistent with PI3K- and PLC-induced PtdIns(4,5) P_2 depletion. Remarkably, TIPE3 overexpression significantly increased the membrane-bound PLC δ -PH-GFP signal in both untreated and PDGF-treated cells, whereas trTIPE3 overexpression greatly decreased it (Figures 5A and S5A). It is important to note that TIPE3 overexpression completely eliminated the PDGF-induced reduction of the membrane-bound PLC δ -PH-GFP signal (vector versus TIPE3 groups), indicating that PtdIns(4,5) P_2 depletion was not significant in the presence of overexpressed TIPE3. The GRP1 and AKT PH domains selectively bind PtdIns(3,4,5) P_3 and PtdIns(3,4,5) P_3 /PtdIns(3,4) P_2 , respectively (Ferguson et al., 2000). In untreated NIH 3T3 cells, AKT-PH-GFP was localized primarily to the cytoplasm and weakly to the nucleus and plasma membrane; GRP1-PH-GFP was localized prominently to the nucleus and weakly to the cytoplasm (Figures 5B and 5C; Figures S5B and S5C). A few minutes after PDGF stimulation, both AKT-PH-GFP and GRP1-PH-GFP showed a noticeable translocation to the plasma membrane. TIPE3 significantly increased the levels of plasma membrane-bound AKT-PH-GFP and GRP1-PH-GFP in both untreated and PDGF-stimulated cells. These TIPE3 effects were dependent on the NT region since the trTIPE3 that lacks it had the opposite effects (Figures 5B and 5C; Figures S5B and S5C).

Although slightly concentrated at the plasma membrane, TIPE3 protein was distributed throughout the cytoplasm of

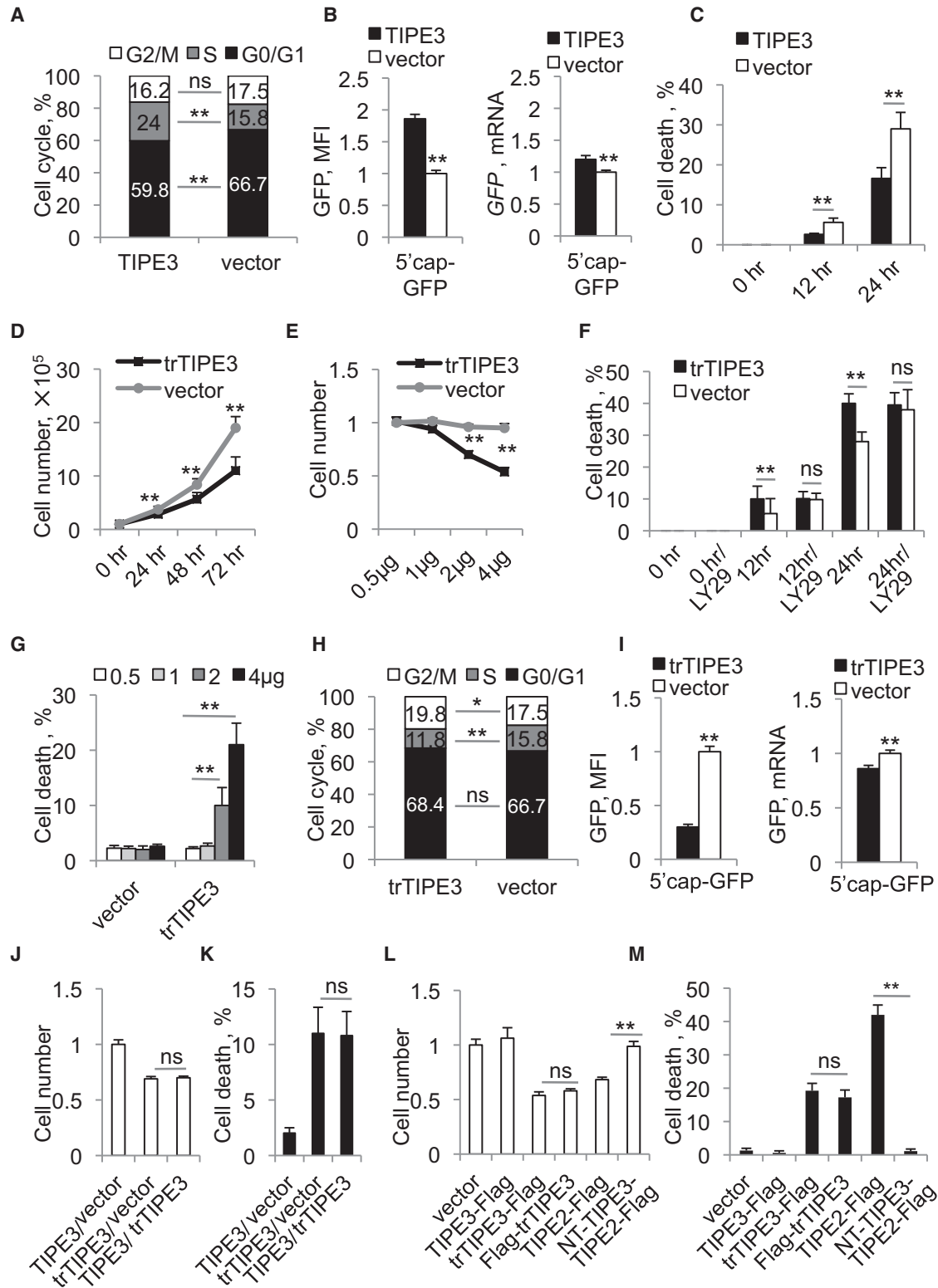


Figure 3. The NT Region of TIPE3 Is Essential for Its Ability to Promote Cell Growth and Survival

(A) Cell cycle analysis of NIH 3T3 cells stably transfected with either TIPE3-Flag or empty vector. (B) 293T cells were cotransfected with pEGFP-C3 (5'cap-GFP, for cap-dependent translation) and either TIPE3-Flag-expressing or empty vector. The relative levels of GFP protein expression 32 hr after transfection were quantified by measuring the cellular mean fluorescence intensity (MFI) (left), whereas the relative levels of GFP mRNA were determined by real-time PCR (right). Protein and mRNA levels of cells transfected with empty vector were set as 1.

(legend continued on next page)

untreated cells (Figure 5D; Figures S5A–S5C). On PDGF activation, TIPE3 protein translocated from cytoplasm to plasma membrane, yielding a clear appearance of plasma membrane localization (Figures 5E and S5A–S5C). No such PDGF-induced effect was seen for the trTIPE3 protein, although a fraction of the protein was also localized to the plasma membrane (Figures 5D and S5A–S5C).

To determine whether altering TIPE3 subcellular localization changes the phosphoinositide distribution, we fused TIPE3 with GFP to force it to go into the nucleus as previously described (Seibel et al., 2007). We found that TIPE3 was excluded from the nucleus, whereas GFP and the TIPE3-GFP fusion protein were present in the nucleus, indicating that GFP confers the ability for TIPE3 to enter this organelle (Figures S5D–S5F). Notably, we observed strong PtdIns(4,5) P_2 staining in the nuclei of all cells expressing TIPE3-GFP but not in those of cells expressing TIPE3 or GFP alone or in nontransfected cells ($p < 0.0001$) (Figures S5D–S5F).

The Crystal Structure of TIPE3 Reveals a Lipid-Binding Scaffold

To help elucidate the molecular mechanism by which TIPE3 functions, we sought to determine its crystal structure. We crystallized the full-length conserved TH domain, i.e., a trTIPE3 that lacks amino acids 2–20, in the space group I222 (Protein Data Bank [PDB] ID: 4Q9V). The structure was determined by molecular replacement, and the atomic model was refined at 2.3 Å resolution (Figure 6A; Table S1).

The structure of the crystallized TIPE3 consists of an NT $\alpha 0$ helix and six additional helices ($\alpha 1$ – $\alpha 6$) that are similar to those observed for TIPE2 (residues 24–184; PDB ID: 3F4M) (Zhang et al., 2009). The helices $\alpha 1$ – $\alpha 6$ of TIPE3 can be aligned to those of TIPE2 with a root-mean-squared deviation (RMSD) of 0.574 Å over 128 aligned C α atoms (Figure 6B). The most prominent feature of the TH fold is the presence of a large centrally located hydrophobic cavity (Figure 6C), which, with 20 Å in depth and 10 Å in diameter, was thought to be the binding site for a lipophilic molecule. Similar to TIPE2 (Zhang et al., 2009), the hydrophobic cavity in TIPE3 is occupied by two tubes of electron density (each measuring approximately 20 Å in length), which

are connected at the surface opening of the cavity (Figure 6D). The shape and size of the electron density are reminiscent of two aliphatic tails of a phospholipid, although the head group cannot be identified because of poor electron density. Notably, positive ion electrospray ionization mass spectrometry of lipids copurified with trTIPE3 from bacteria revealed two major peaks: 653 mass-to-charge ratio and 683 mass-to-charge ratio. The molecular mass of the first peak is indicative of 16:0/16:1 phosphatidic acid (PA), whereas that of the second peak is indicative of 16:0/18:0 or 16:0/18:1 PA. Therefore, it is likely that PAs are the phospholipids that occupy the hydrophobic cavity of trTIPE3 expressed in bacteria (which do not possess phosphoinositides).

Within the same asymmetric unit, helix $\alpha 0$ from one TIPE3 molecule forms a coiled coil with that of another TIPE3 molecule, constituting a homodimer (Figure S6A). These two α helices interact with each other mainly through van der Waals contacts. In addition, the $\alpha 0$ helix from one TIPE3 molecule also interacts with the $\alpha 1$ helix of its partner molecule. Notably, truncation of the $\alpha 0$ helix exhibits no significant effect on the elution profile of TIPE3 on gel filtration, suggesting that the observed TIPE3 dimer is likely an artifact of crystallization at high protein concentrations.

TIPE3 Binds to Phosphoinositides through Its TH domain, and This Binding Is Essential for Its Function

Next, we examined whether affinity-purified TIPE3 exhibits any binding specificity for the various eukaryotic lipid molecules in the protein-lipid overlay assay (Figures S6B–S6D). Of the 22 different types of eukaryotic lipids tested, TIPE3 appeared to predominantly interact with PtdIns(4,5) P_2 , PtdIns(3,5) P_2 , PtdIns(3,4) P_2 , PtdIns4 P , PtdIns(3,4,5) P_3 , and PA (Figures S6C and S6D; data not shown). The trTIPE3, as well as TIPE2, TIPE1, and TNFAIP8 proteins, interacted with the same set of lipids, indicating that the highly conserved TH domain, but not the NT region, is responsible for the observed lipid binding activity (Figures S6B, S6C, and S6E). By contrast, the PLC δ -PH domain (GST-PLC δ -PH) interacted only with PtdIns(4,5) P_2 in the same assay (Figure S6C). PLC δ -PH binds to the PtdIns(4,5) P_2 head group, and addition of 15 μ M free Ins(1,4,5) P_3 to the overlay assay was sufficient to prevent PLC δ -PH binding to

(C) NIH 3T3 cells stably transfected with either TIPE3-Flag or empty vector were cultured in serum-free medium for the indicated times, and cell death was assessed by trypan blue staining.

(D) Cell growth of NIH 3T3 cells stably transfected with either trTIPE3-Flag or empty vectors over indicated times.

(E) Relative numbers of 293T cells transfected with the indicated amounts of trTIPE3-Flag plasmid or empty vector were determined 32 hr after transfection. Number of 293T cells transfected with 0.5 μ g of empty vector was set as 1.

(F) NIH 3T3 cells stably transfected with either trTIPE3-Flag or empty vectors were cultured in serum-free medium with or without LY29 (LY29004) for the indicated times. Cell death was assessed by trypan blue staining.

(G) Cell death of 293T cells transfected with the indicated amounts of trTIPE3-Flag plasmid or empty vector were assessed by trypan blue staining.

(H) Cell cycle analysis of NIH 3T3 cells stably transfected with either trTIPE3-Flag or empty vectors.

(I) 293T cells were cotransfected with pEGFP-C3 and either trTIPE3-Flag-expressing or empty vectors. The relative levels of GFP protein expression 16 hr after transfection were quantified by measuring cellular MFI, whereas the relative levels of the GFP mRNA expression were determined by real-time PCR. Protein and mRNA levels of cells transfected with empty vector were set as 1.

(J and K) 293T cells were cotransfected with equal amounts (2 μ g) of the following plasmids as indicated: empty, TIPE3-Flag-expressing, or trTIPE3-Flag-expressing vectors. Relative cell numbers were determined (J), and the degree of cell death (K) was assessed by trypan blue staining 32 hr later. For (J), the number of 293T cells transfected with empty vector was set as 1.

(L and M) 293T cells were transfected with one of the following plasmids as indicated: empty vector, TIPE3-Flag, trTIPE3-Flag, Flag-trTIPE3, TIPE2-Flag, NT-TIPE3-TIPE2-Flag (TIPE2-Flag fused with the NT region of TIPE3). Relative cell numbers were determined (L), and the degree of cell death (M) was assessed by trypan blue staining 32 hr later. For (L), the number of 293T cells transfected with empty vector was set as 1.

The y axis values represent means \pm SD. * $p < 0.05$; ** $p < 0.01$; ns, not significant. The experiments were performed in duplicates and repeated at least three times with similar results. See also Figure S3.

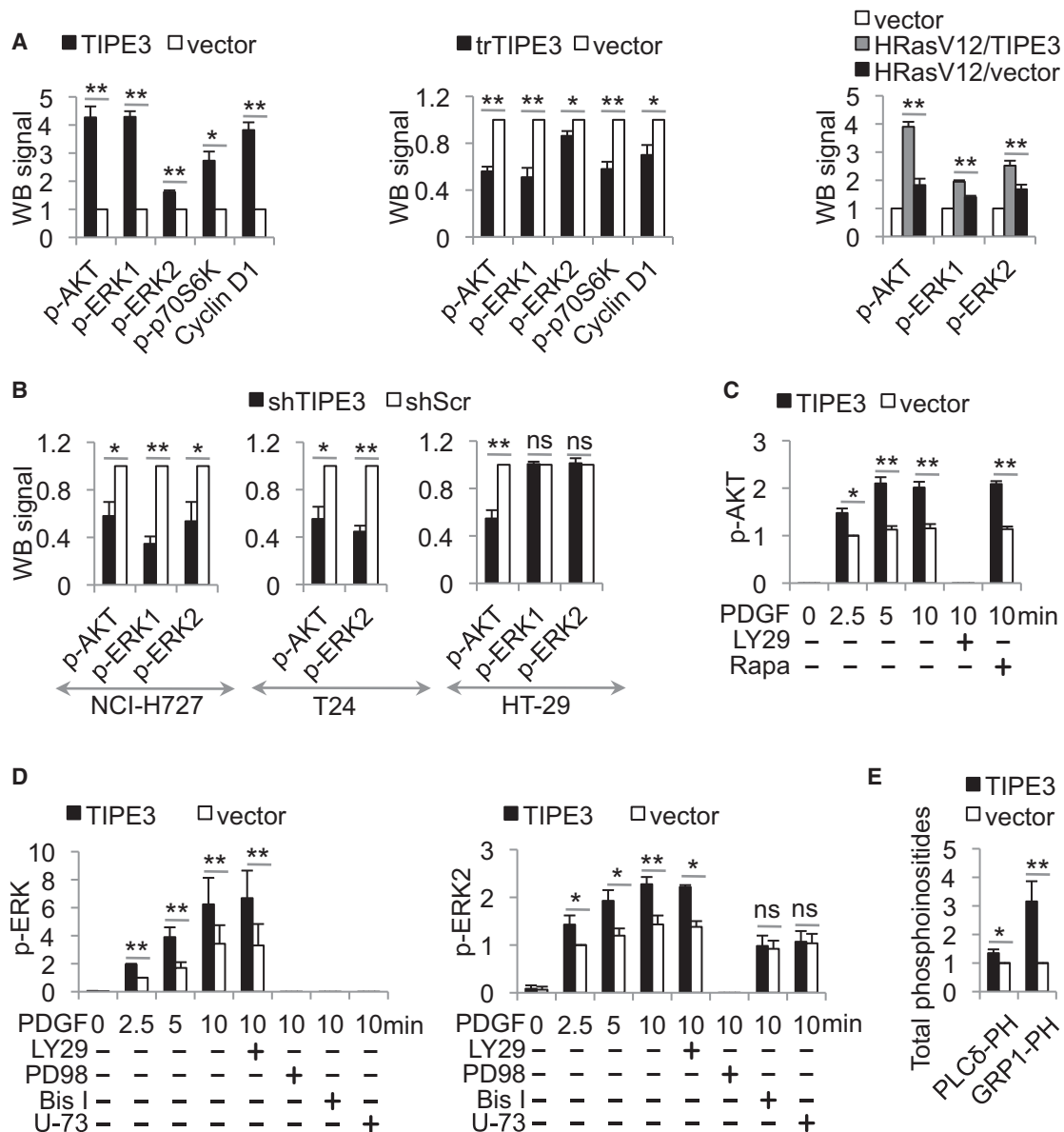


Figure 4. TIPE3 Promotes the Activation of PI3K-AKT and MEK-ERK Pathways

(A) Whole cell lysates were prepared from NIH 3T3 cells stably transfected with TIPE3-Flag, trTIPE3-Flag, or empty vectors (left and middle panels), or TIPE3-Flag and/or HRasV12 vectors (right panel). Western blot (WB) was performed using antibodies against the indicated proteins. The densitometric quantification of protein signals was made using ImageJ software. Signals of cells transfected with empty vector were set as 1.

(B) Whole cell lysates were prepared from NCI-H727, T24, and HT-29 cells stably expressing either shTIPE3 or small hairpin scrambled (shScr). Western blot (WB) was performed using antibodies against the indicated proteins. Signals of cells treated with shScr were set as 1.

(C and D) NIH 3T3 cells stably transfected with either TIPE3-Flag or empty vectors were serum starved and then stimulated with 40 ng/ml of PDGF for the indicated times, with or without the following inhibitors: LY29 (LY29004), Rapa (Rapamycin), PD98 (PD98059), Bis I (Bisindolylmaleimide I), or U-73 (U-73122). (C) pertains to p-AKT, and (D) pertains to p-ERK. Lysates of these cells were used for western blot with antibodies against the indicated proteins. Signals of cells transfected with vector 2.5 min after PDGF stimulation were set as 1.

(E) Cellular levels of PtdIns(4,5)P₂ and PtdIns(3,4,5)P₃ in NIH 3T3 cells stably transfected with either TIPE3-Flag or empty vector were estimated by protein-lipid overlay assay with GST-PLCδ-PH and GST-GRP1-PH domains as described in [Supplemental Experimental Procedures](#). Signals of cells transfected with empty vector were set as 1.

The y axis values represent means ± SD. *p < 0.05, and **p < 0.01; ns, denotes not significant. The abbreviation p- indicates phosphorylated. The experiments were performed at least three times with similar results. See also [Figure S4](#).

nitrocellulose-bound PtdIns(4,5)P₂ (Figure S6C). However, adding free Ins(1,4,5)P₃ had no effect on TIPE3 binding to PtdIns(4,5)P₂, suggesting that the mode of interaction is different from that

between PLCδ-PH and PtdIns(4,5)P₂ (Figure S6C). This is consistent with our structural data, which identify an anchoring role for the acyl chains of phospholipid (Figure 6D).

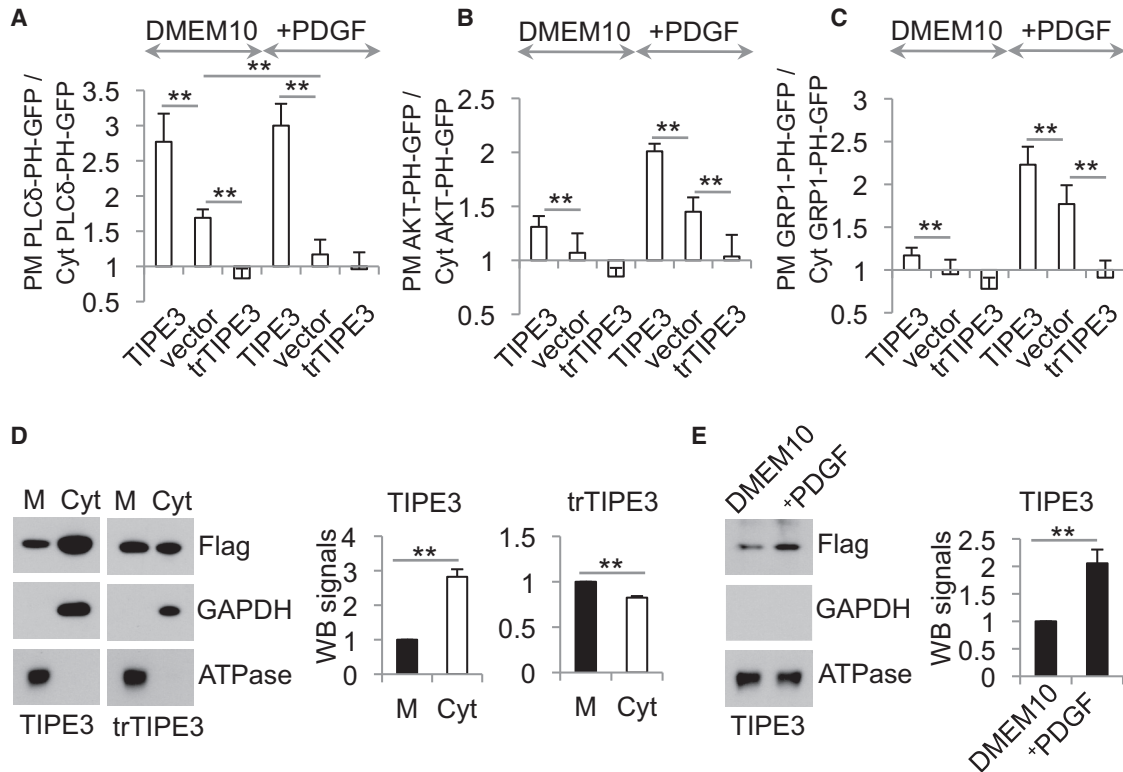


Figure 5. TIPE3 Regulates Lipid Metabolism and Signaling

(A–C) NIH 3T3 cells were cotransfected with PLCδ-PH-GFP (A), AKT-PH-GFP (B), or GRP1-PH-GFP (C) and one of the following plasmids as indicated: pRK5 vector (vector), pRK5-TIPE3-Flag (TIPE3), and pRK5-trTIPE3-Flag (trTIPE3). Thirty-two hours after the transfection, cells were cultured in Dulbecco’s modified Eagle’s medium (DMEM) with 10% fetal calf serum (DMEM10, in A through C) or in DMEM10 with 40 ng/ml of PDGF for 5.5 min (*PDGF in A), or they were serum starved for 4 hr and then cultured in DMEM containing 40 ng/ml of PDGF for 7.5 min (*PDGF in B and C) followed by fixation. Cells expressing the Flag-tagged proteins were selected by immunofluorescence microscopy with an anti-Flag antibody. Ratios of GFP fluorescence intensity on plasma membrane (PM) over that in the cytoplasm (Cyt) of the same cells are calculated based on line fluorescence intensity profiles.

(D) Membrane (M) and cytoplasmic (Cyt) proteins fractions were prepared from NIH 3T3 cells stably transfected with TIPE3-Flag and trTIPE3-Flag. Western blot (WB) was performed using antibodies against the indicated proteins. Signals of TIPE3 or trTIPE3 in membrane fractions were set as 1.

(E) NIH 3T3 cells stably transfected with TIPE3-Flag were cultured in DMEM with 10% of FCS (DMEM10) or serum-starved for 4 hr and then cultured in DMEM containing 40 ng/ml of PDGF for 7.5 min (*PDGF). Membrane protein fractions (M) of these cells were analyzed by western blot (WB) using antibodies against the indicated proteins. Signals of TIPE3 in membrane fractions of cells cultured in DMEM10 were set as 1.

Values represent means ± SD; **p < 0.01. The experiments were repeated at least three times with similar results. See also Figure S5.

To test the importance of the hydrophobic cavity in the TIPE3 TH domain, we replaced leucine 60, positioned in the center of this pocket, with the much bulkier tryptophan to yield the TIPE3 60W mutant (Figure S7A). A similar approach was described to test the importance of the hydrophobic cavity in orphan nuclear hormone receptors hypothesized to bind phosphoinositides (Krylova et al., 2005; Sablin et al., 2003). TIPE3 60W mutant showed markedly reduced ability to bind phosphoinositide (Figure S7B). This finding is consistent with the structure-based proposition that the acyl chains of phosphoinositide are positioned inside the TH domain cavity, allowing the negatively charged head group to form electrostatic interactions with the neighboring positively charged side chains that line the opening of the cavity (Figures 6C and 6D). Supporting this analysis, a TIPE3 4Q mutant (in which lysines 33, 34, 38, and 42 were all replaced with glutamines) and a TIPE3 2Q mutant (in which arginines 93 and 109 were replaced with glutamines) both exhibited marked reductions in phosphoinositide binding

(Figures S7A and S7B). By contrast, a TIPE3 3Q mutant—in which glutamine replaces lysines 76, 79, and 83, which lie on a positively charged surface distant from the cavity opening—showed WT levels of phosphoinositide binding in the overlay assay (Figures S7A and S7B).

Notably, the TIPE3 mutants that showed impaired phosphoinositide binding also had markedly reduced TIPE3 functions. Compared with WT TIPE3, the TIPE3 60W, 2Q, and 4Q mutants had significantly reduced capacities to promote cap-dependent translation of GFP (Figure S7C), whereas TIPE3 3Q (which retains phosphoinositide binding) did not—although all mutants were expressed at similar levels as those of the WT TIPE3 (Figures S7C and S7D). As expected, TIPE3 4Q had no detectable effects on ERK activation or PtdIns(4,5)P₂ levels and might even reduce the levels of AKT phosphorylation and PtdIns(3,4,5)P₃ (Figures S7E and S7F). Introduction of a 4Q-equivalent mutation in trTIPE3 abolished its ability to bind phosphoinositide (Figure S7B). Moreover, 4Q, 2Q, and 60W

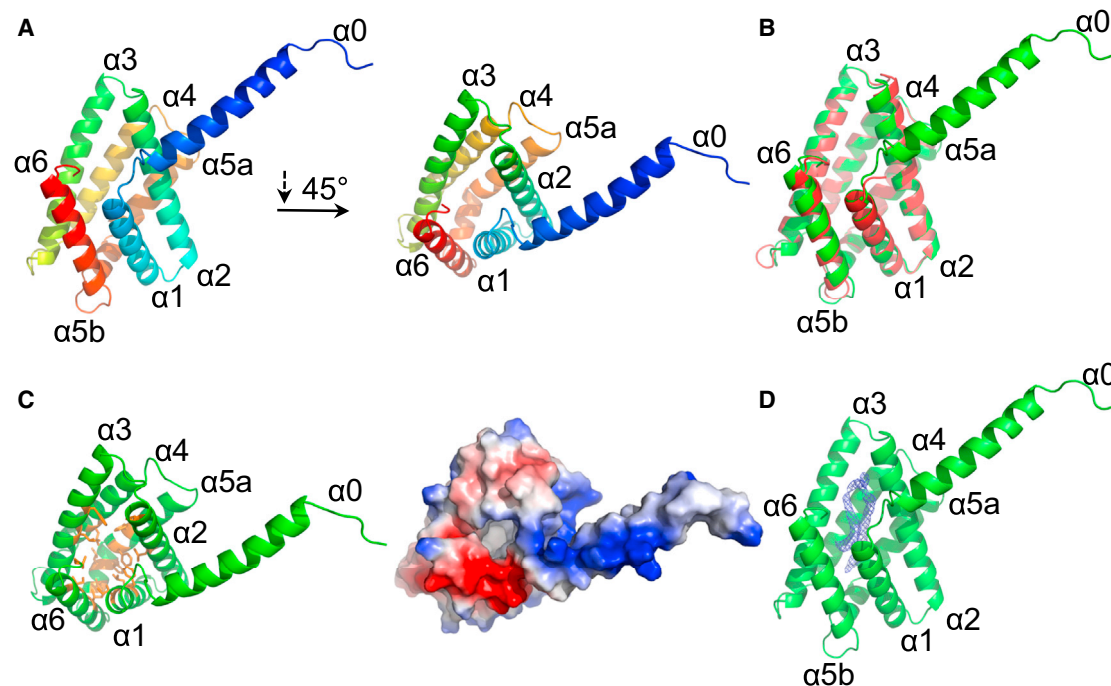


Figure 6. The Crystal Structure of the TH-Domain of Human TIPE3

(A) Cartoon presentation of TH-domain of human TIPE3 (trTIPE3, residues 21–204). Helices are rainbow colored with $\alpha 0$ in blue and $\alpha 6$ in red. (B) Cartoon representation of superposition of human TIPE3 (residues 21–204, shown in green) with the human TIPE2 (residues 24–184, shown in red) structures. (C) TIPE3 contains a centrally located hydrophobic cavity. (Left) TIPE3 is shown in a green cartoon representation; amino acids with hydrophobic side chains that line the cavity are shown in orange. (Right) TIPE3 electrostatic surface potential: blue, positive; red, negative. (D) TIPE3 is shown in a green cartoon representation. The two long connected tubes of 2Fo-Fc electron density found in TIPE3 cavity is shown in blue mesh, contoured at 1.5 σ . See also [Table S1](#) and [Figure S6](#).

mutations in trTIPE3 reduced its ability to inhibit cell proliferation and to induce cell death ([Figures S7G–S7I](#)), whereas the 3Q mutation had no such effect.

TIPE3 Can Act as a PtdIns(4,5) P_2 and PtdIns(3,4,5) P_3 Transfer Protein

Although the TH fold is unique, the lipid-binding mode by the TIPE family of proteins is reminiscent of lipid-binding mode by lipid transfer proteins ([Prinz, 2010](#)). We wondered whether phosphoinositide-loaded TIPE3 might exert its effects in part by transferring phosphoinositides to the plasma membrane and whether the dominant negative trTIPE3 might promote cell death by reducing the membrane pool of PtdIns(4,5) P_2 and PtdIns(3,4,5) P_3 . Consistent with this notion, trTIPE3-induced cell death could be partially reversed by overexpressing a myristoylated variant of phosphatidylinositol-4-phosphate 5-kinase (PIP5K) that leads to elevated plasma membrane PtdIns(4,5) P_2 ([Figure S7J](#)) ([Volpicelli-Daley et al., 2010](#); [Wang et al., 2008](#)). Neither a constitutively active PI3K (PI3KCAE545) nor HRasV12 had any detectable effect on trTIPE3-induced cell death ([Figure S7J](#)).

To determine whether WT TIPE3 protein might have properties consistent with a phosphoinositide transfer protein, we examined whether it could recognize PtdIns(4) P , PtdIns(4,5) P_2 , and PtdIns(3,4,5) P_3 present in a lipid bilayer, and extract the lipid

from the membrane. We purified recombinant TIPE3 and TIPE3 4Q from mammalian cells ([Figure S6B](#)) and assessed their binding to small unilamellar vesicles (SUVs) containing 100% phosphatidylcholine (PC), 10% PtdIns(4) P , 10% PtdIns(4,5) P_2 , or 10% PtdIns(3,4,5) P_3 in a PC background using a well-established centrifugation-based assay ([Kavran et al., 1998](#); [Lee and Lemmon, 2001](#)). TIPE3 sedimented efficiently with vesicles containing 10% phosphoinositides, with the following order of preference: PtdIns(3,4,5) P_3 > PtdIns(4,5) P_2 > PtdIns(4) P ([Figures 7A and 7B](#)). Consistent with the results of the overlay assay, TIPE3 4Q showed significantly reduced binding to PtdIns(4,5) P_2 - and PtdIns(3,4,5) P_3 -containing vesicles compared with WT TIPE3; more than 60% of the 20 μ M TIPE3 and only ~30% of 20 μ M TIPE3 4Q were bound to vesicles when the concentration of vesicles was 1,000 μ M ([Figures 7A and 7B](#)). Lack of binding specificity of TIPE3 4Q to PtdIns(4) P -, PtdIns(4,5) P_2 -, and PtdIns(3,4,5) P_3 -containing vesicles suggests that lysines in the $\alpha 0$ helix may form electrostatic interactions with 5- and 3-phosphate groups of PtdIns(4,5) P_2 and PtdIns(3,4,5) P_3 . By contrast, only background levels of TIPE3 and TIPE3 4Q sedimented with 100% PC vesicles. A negative control protein (trypsin inhibitor) showed no binding to either type of vesicles ([Figures 7A and 7B](#)).

Having established that TIPE3 could bind to vesicles containing PtdIns(4,5) P_2 , we next asked whether the protein could

extract fluorescently labeled phosphoinositide from these vesicles and effectively solubilize it. When increasing concentrations of TIPE3 were incubated for 1 hr with 100 μ M vesicles containing 20% TopFluor PtdIns(4,5) P_2 and 80% PC, substantial amounts of TopFluor PtdIns(4,5) P_2 fluorescence was detected in the supernatant after ultracentrifugation, whereas equivalent experiments with the PLC δ -PH domain showed no significant fluorescence in the supernatant (Figures 7C and S6B). This result suggests that TIPE3 can effectively remove PtdIns(4,5) P_2 from the vesicles and solubilize it in the aqueous phase—extracting up to 50% of the total available PtdIns(4,5) P_2 at a protein concentration of 40 μ M. Size exclusion chromatographic analysis of the supernatants revealed a single peak corresponding to TIPE3 monomer, ruling out the possibility that TIPE3/vesicle complexes remain in the supernatants (data not shown). Supporting its dominant negative effect, trTIPE3 did not remove TopFluor PtdIns(4,5) P_2 after binding to 20% TopFluor PtdIns(4,5) P_2 -containing vesicles; \sim 10% of 20 μ M trTIPE3 remained in supernatant (Figure S7K). Similar to trTIPE3, TIPE2 strongly bound to vesicles containing 20% PtdIns(4,5) P_2 and 80% PC, with only \sim 15% remaining unbound (data not shown). It is important to note that neither TIPE3 nor TIPE3 4Q was able to bind and extract TopFluor PC from 100 μ M vesicles containing 20% TopFluor PC and 80% PC used as control (Figure S7K).

We further investigated the ability of TIPE3 to extract PtdIns(4,5) P_2 from membranes using a surface plasmon resonance (SPR)-based assay. PtdIns(4,5) P_2 -containing vesicles (3% and 10%) were immobilized on L1 sensor chips, and the binding signal obtained with a saturating injection of PLC δ -PH was measured before and after TIPE3 or TIPE3 4Q had been flowed over the sensor chip. A significant reduction (more than 60%) in PLC δ -PH binding at saturation was detected after TIPE3 had been exposed to the sensor chip (Figure 7D), indicating that TIPE3 extracts PtdIns(4,5) P_2 from the immobilized vesicles. TIPE3 4Q also appeared to extract PtdIns(4,5) P_2 from the immobilized membranes, but to a reduced extent, which is consistent with our other studies of this mutant (Figure 7D).

As discussed earlier, TIPE3 overexpression appears to increase both total and plasma membrane levels of PtdIns(4,5) P_2 in NIH 3T3 cells. To determine whether TIPE3 is capable of inserting extracted PtdIns(4,5) P_2 into a lipid bilayer, we analyzed transfer of TopFluor PtdIns(4,5) P_2 from the soluble TIPE3/TopFluor PtdIns(4,5) P_2 complexes detected in the supernatant in Figure 7C to 100% PC vesicles. We collected supernatants from mixtures of TIPE3 with 100 μ M TopFluor PtdIns(4,5) P_2 -containing vesicles that had been subjected to ultracentrifugation and incubated them with vesicles containing 250 μ M 100% PC for 1 hr at room temperature. The mixtures were then recentrifuged as described elsewhere (Lee and Lemmon, 2001), and the level of TopFluor PtdIns(4,5) P_2 fluorescence remaining in the supernatant was measured. Addition of vesicles containing 100% PC alone led to a substantial reduction in fluorescence corresponding to presumed TIPE3/TopFluor PtdIns(4,5) P_2 complexes in the supernatant (Figure 7E). This was accompanied by a dramatic increase in fluorescence intensity associated with the vesicle pellet (Figure 7F), indicating that TopFluor PtdIns(4,5) P_2 was transferred into the PC vesicles. The concomitant loss of TopFluor PtdIns(4,5) P_2 -derived fluorescence from the supernatant and its acquisition in the pellet was not accompanied by

any change in TIPE3 protein concentrations in the supernatant, arguing that TIPE3 has transferred the labeled PtdIns(4,5) P_2 to the PC vesicles (Figure 7E).

TIPE3 Can Promote the Generation of PtdIns(3,4,5) P_3 by PI3K

To examine whether TIPE3 could promote the phosphorylation of PtdIns(4,5) P_2 by PI3K(p110 α /p85 α), we performed in vitro membrane capture (enzymatic) assay for the PI3K in the absence or presence of increasing amounts of TIPE3 (Knight et al., 2007). SUVs containing 10% PtdIns(4,5) P_2 in a PC background were used in this assay. We found that TIPE3 indeed stimulated PI3K activity in a concentration-dependent manner (Figure 7G). At 20 min after the initiation of the PI3K assay, we observed three times more PtdIns(3,4,5) P_3 in reactions containing 200 nM TIPE3, two times more PtdIns(3,4,5) P_3 in reactions containing 100 nM TIPE3, and 1.65 times more PtdIns(3,4,5) P_3 in reactions containing 20 nM TIPE3 than those of control PI3K reactions lacking TIPE3 (BSA was used as a control protein). Finally, we examined whether TIPE3 associated with PI3K. We immunoprecipitated endogenous p110 α , p110 β , and p85 from NIH 3T3 cells overexpressing TIPE3, with or without PDGF treatment, and found that TIPE3 did not coimmunoprecipitate with these PI3K proteins. In addition, we did not detect an association of TIPE3 with the oncogenic mutant of p110 α , E545K, when both proteins were overexpressed in 293T cells.

DISCUSSION

PtdIns transfer proteins (PITPs) play essential roles in phospholipid signaling, and their dysregulation leads to a variety of disorders, including cancer and degenerative diseases (Nile et al., 2010). It is unclear whether, and to what degree, currently known PITPs or PITP-like proteins can transfer phosphoinositides. It was reported that the yeast Kes1/Osh4p protein (de Saint-Jean et al., 2011) and the human α -TTP protein (Kono et al., 2013) that belongs to the Sec14-like family might transfer PtdIns4P and PtdIns(4,5) P_2 , respectively, but not other phosphoinositides. The mammalian nuclear receptor SF-1 and LRR-1 proteins of the NR5A family were also found to accommodate phosphoinositides within their large hydrophobic cavities (Krylova et al., 2005), but whether they can transfer these lipids is unknown.

The results reported here argue that the TH domain of TIPE proteins can function as a lipid transfer domain and that TIPE3 is a lipid transfer protein for two second messengers, PtdIns(4,5) P_2 and PtdIns(3,4,5) P_3 . Crystal structure and mutagenesis analyses revealed that the acyl chains of lipid are likely accommodated in the hydrophobic cavity formed by the α 1– α 6 helices of the TIPE3 TH domain. The negatively charged head group of phosphoinositides is likely involved in electrostatic interactions with positively charged amino acids of the α 0 helix (that might function as a flexible “lid”) and those located at the entrance to the hydrophobic cavity. Structure determination of the full-length TIPE3 bound to phosphoinositides is required to provide additional insight into this issue.

Our results support a dual role model for TIPE3 in phosphoinositide signaling and metabolism. TIPE3 may regulate the spatial and temporal distribution of lipid second messengers in

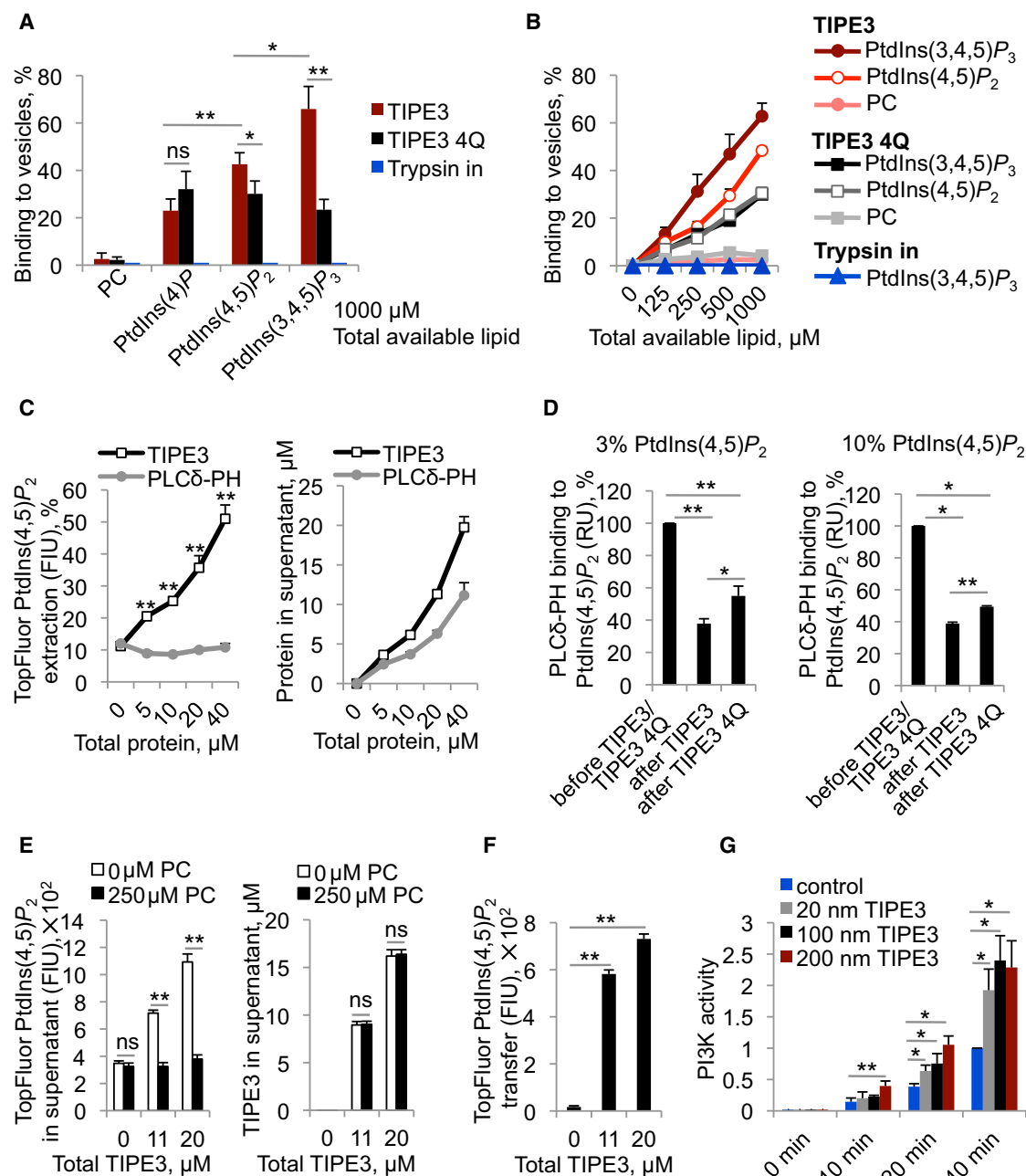


Figure 7. TIPE3 Is a Phosphoinositide Transfer Protein

(A and B) The sedimentation-based binding assay was used to determine the percentages of TIPE3, TIPE3 4Q, and control protein trypsin inhibitor (Trypsin in) bound to vesicles containing 10% PtdIns(4)P + 90% PC (10% PtdIns(4)P); 10% PtdIns(3,4,5)P₃ + 90% PC (10% PtdIns(3,4,5)P₃); 10% PtdIns(4,5)P₂ + 90% PC (10% PtdIns(4,5)P₂); or 100% PC as indicated. (A) Binding with 1,000 μM concentration of total lipid; (B) binding with varying concentrations of total lipid. Proteins were used at a concentration of 20 μM.

(C) The sedimentation-based extraction assay was used to determine the percentages of TopFluor PtdIns(4,5)P₂ extracted from 100 μM 20% TopFluor PtdIns(4,5)P₂ + 80% PC vesicles and transferred to supernatant by TIPE3 and PLCδ-PH (left panel); and fractions of TIPE3 and PLCδ-PH proteins not bound to the 20% TopFluor PtdIns(4,5)P₂ + 80% PC vesicles (right panel).

(D) In the SPR-based assay, 3% (left panel) and 10% (right panel) PtdIns(4,5)P₂-containing vesicles were immobilized on L1 sensor chips, and the binding signal obtained with a saturating injection of GST-PLCδ-PH (5 μM) was measured before and after TIPE3 or TIPE3 4Q (both at 40 μM) had been flowed over the sensor chip. GST-PLCδ-PH binding to PtdIns(4,5)P₂-containing surfaces before TIPE3 or TIPE3 4Q exposure is set as 100%, and GST-PLCδ-PH binding to PtdIns(4,5)P₂-containing surfaces after TIPE3 or TIPE3 4Q exposure is presented as the percentage reduction.

(E) The sedimentation-based transfer assay was used to measure the depletion of TopFluor PtdIns(4,5)P₂ from soluble TIPE3-TopFluor PtdIns(4,5)P₂ in supernatants (left panel) and fractions of TIPE3 remaining in supernatants (right panel) after incubation with 100% PC vesicles or buffer alone.

(legend continued on next page)

response to external or internal stimuli by sequestering PtdIns(4,5) P_2 and PtdIns(3,4,5) P_3 from the lipid bilayer and shuttling them through the aqueous phase. Additionally, TIPE3 may also function as a lipid-presenting protein to enhance the activity of phosphoinositide-modifying enzymes such as PI3K. A similar function has been reported for PtdIns transfer proteins such as Sec14, the major yeast PITP protein that regulates phosphoinositide signaling and metabolism by presenting PtdIns to PI4K (Bankaitis et al., 2010; Lev, 2010; Prinz, 2014; Schaaf et al., 2008). Consistent with this view, TIPE3 physically translocates from cytoplasm to plasma membrane on cell activation by PDGF or on cell transformation by the oncogenic HRasV12 (data not shown). Upregulation of TIPE3 expression in PDGF-stimulated cells and cancer cells may positively feed back to cell activation through the aforementioned mechanism.

The TIPE3 TH domain is highly homologous to TH domains of other members of the TIPE family. The domain is also highly conserved through evolution and is found in vertebrates; invertebrates such as the mosquito and fruit fly; and unicellular eukaryotes such as choanoflagellate, Dictyostelium, and Entamoeba. This raises the question as to whether all TH domains are involved in regulating lipid signaling. Our studies indicate that all murine TIPE family proteins bind phosphoinositides, and, in addition to TIPE3, TIPE2 regulates the PtdIns(3,4,5) P_3 signaling pathway. However, the functions of TH domains may be regulated by other sequences present in the protein. For example, as reported here, the TIPE3 NT region, which is not shared by other members of the family, is essential for the effects seen on cell growth and survival; TIPE3 lacking the NT region functions in a dominant negative fashion. Similarly, some TH-containing proteins of the unicellular eukaryotes possess NT PH domains, which likely affect their functions. Therefore, TH-containing proteins may play diverse roles depending on the non-TH sequences that they also possess. Thus, despite their high sequence homology in the TH domains, TIPE2 and TIPE3 appear to play distinct roles. TIPE2 functions as a negative regulator of neoplastic cell growth, and its expression is downregulated during liver carcinogenesis. The tumor suppressor activity of TIPE2 is likely dependent on its interaction with Rac1 and Rgl/RalGDS molecules (Gus-Brautbar et al., 2012; Wang et al., 2012). However, no such interaction could be found for TIPE3 (data not shown). Therefore, TIPE2 and TIPE3 appear to have distinct molecular mechanisms.

Hyperactivation of PtdIns(3,4,5) P_3 signaling is reported in more than 50% of human cancers. Somatic gene mutations of the signaling molecules such as PTEN and PI3K are found in many of these cancers. Our findings reveal a mechanism of hyperactivating PtdIns(3,4,5) P_3 signaling pathway in cancer cells by TIPE3, a phosphoinositide transfer protein. Therefore, TIPE3 may represent a therapeutic target for treating malignant diseases.

EXPERIMENTAL PROCEDURES

Mice

Male athymic nude mice (*nu/nu*) and WT C57BL/6 mice were purchased from Jackson Laboratories. *Tipe3*^{+/-} C57BL/6 mice (Tnfaip8l3^{tm1a(KOMP)Mbp}) were purchased from the Knockout Mouse Project Repository. Mice were housed in the University of Pennsylvania Animal Care Facilities under pathogen-free conditions. All animal procedures were preapproved by the Institutional Animal Care and Use Committee of the University of Pennsylvania, and all experiments conform to the relevant regulatory standards.

Human Samples

Human non-small cell lung cancer arrays containing 60 tumor samples and their corresponding adjacent normal tissues, as well as human esophageal carcinoma arrays containing 24 tumor samples and their adjacent normal tissues, were purchased from Outdo Biotech. Human colon cancer and cervical cancer microarrays were purchased from Xi'an Alena Biotech. All samples have been deidentified prior to analysis and are therefore considered exempt. All human study procedures were preapproved by the Institutional Review Board of Shandong University.

Crystallization, Data Collection, and Structure Determination

The human trTIPE3 (residues 21–204) was purified as described in Supplemental Experimental Procedures. Crystals of trTIPE3 were grown at 18°C using the hanging-drop vapor diffusion method by mixing 1 μ l of protein (10 mg/ml in 25 mM Tris-HCl, 1 M NaCl, pH 8.0) with 1 μ l of reservoir solution (0.1 M MES 6.7, 1.95 M (NH₄)₂SO₄). The crystals appeared in 2 days and grew to full size in a week. The 2.3 Å native data were collected at Shanghai Synchrotron Radiation Facility beamline BL17U. The data sets were integrated and scaled using the HKL2000 package. Further processing was performed using the CCP4 suite. The structure was solved by molecular replacement using PHASER and manually refined with COOT and PHENIX. Data collection and refinement statistics are listed in Table S1. All the figures were prepared using PyMOL software.

Other experimental procedures, including in vivo tumorigenesis studies; human tumor studies; cell culture; protein purification; protein crystallization; protein-lipid overlay assay; and phosphoinositide binding, extraction, and transfer assays are available in Supplemental Information.

ACCESSION NUMBERS

The TIPE3 structure data were deposited in the PDB with the ID code of 4Q9V.

SUPPLEMENTAL INFORMATION

Supplemental Information includes Supplemental Experimental Procedures, seven figures, and one table and can be found with this article online at <http://dx.doi.org/10.1016/j.ccr.2014.07.025>.

AUTHOR CONTRIBUTIONS

S.A.F. and Y.H.C. conceived the study and wrote the article. S.A.F. designed and performed the experiments and analyzed the data. C.L.O., A.V., T.C., Z.W., and H.S. were involved in the design or execution of several experiments. M.A.L. made suggestions for the design of the lipid biochemical studies and contributed to manuscript preparation. X.L., L.Z., J.C., and S.L. designed and performed the human tumor studies. J.W. and Y.S. solved the crystal

(F) The sedimentation-based transfer assay was used to monitor the transfer of TopFluor PtdIns(4,5) P_2 from soluble TIPE3-TopFluor PtdIns(4,5) P_2 in supernatants to 100% PC vesicles.

(G) Time course of PI3K (p110 α /p85 α)-mediated phosphorylation of PtdIns(4,5) P_2 in the absence or presence of TIPE3 at indicated concentrations. The levels of PtdIns(3,4,5) P_3 were measured by protein-lipid overlay assay with GST-GRP1-PH domain. PI3K activity determined at 40 min in the absence of TIPE3 was set to 1. FIU, fluorescence intensity units; RU, resonance units. Values represent means \pm SD. * $p < 0.05$; ** $p < 0.01$; ns, not significant.

For (A)–(F), the experiments were repeated at least three times with similar results. For (G), the experiments were performed in triplicates and repeated two times with similar results. See also Figure S7.

structure of TIPE3 and contributed to manuscript preparation. Y.H.C. oversaw the project.

ACKNOWLEDGMENTS

We thank Thomas Porturas, George Luo, Qingguo Ruan, Derek Johnson, Yael Gus-Brautbar, Xiaohong Liang, and Fumin Shi for conceptual inputs and technical assistance. We are grateful to Jeannine Mendrola for providing purified PLC δ -PH and Katarina Moravcevic for providing purified GST-PLC δ -PH and technical assistance. This work was funded by the NIH (grants AI-077533, AI-050059, and GM-085112 to Y.H.C.), the National Natural Science Foundation of China (projects 31130002 and 31021002 to Y.S.), and the Ministry of Science and Technology (grant numbers 2009CB918801 to Y.S. and 2011CB503906 to L.Z.).

Received: January 24, 2014

Revised: April 29, 2014

Accepted: July 28, 2014

Published: September 18, 2014

REFERENCES

- Ahn, S.H., Deshmukh, H., Johnson, N., Cowell, L.G., Rude, T.H., Scott, W.K., Nelson, C.L., Zaas, A.K., Marchuk, D.A., Keum, S., et al. (2010). Two genes on A/J chromosome 18 are associated with susceptibility to *Staphylococcus aureus* infection by combined microarray and QTL analyses. *PLoS Pathog.* **6**, e1001088.
- Bankaitis, V.A., Mousley, C.J., and Schaaf, G. (2010). The Sec14 superfamily and mechanisms for crosstalk between lipid metabolism and lipid signaling. *Trends Biochem. Sci.* **35**, 150–160.
- de Saint-Jean, M., Delfosse, V., Douguet, D., Chicanne, G., Payrastra, B., Bourguet, W., Antonny, B., and Drin, G. (2011). Osh4p exchanges sterols for phosphatidylinositol 4-phosphate between lipid bilayers. *J. Cell Biol.* **195**, 965–978.
- Ferguson, K.M., Kavran, J.M., Sankaran, V.G., Fournier, E., Isakoff, S.J., Skolnik, E.Y., and Lemmon, M.A. (2000). Structural basis for discrimination of 3-phosphoinositides by pleckstrin homology domains. *Mol. Cell* **6**, 373–384.
- Fruman, D.A., Meyers, R.E., and Cantley, L.C. (1998). Phosphoinositide kinases. *Annu. Rev. Biochem.* **67**, 481–507.
- Gus-Brautbar, Y., Johnson, D., Zhang, L., Sun, H., Wang, P., Zhang, S., Zhang, L., and Chen, Y.H. (2012). The anti-inflammatory TIPE2 is an inhibitor of the oncogenic Ras. *Mol. Cell* **45**, 610–618.
- Hitomi, J., Christofferson, D.E., Ng, A., Yao, J., Degterev, A., Xavier, R.J., and Yuan, J. (2008). Identification of a molecular signaling network that regulates a cellular necrotic cell death pathway. *Cell* **135**, 1311–1323.
- Kavran, J.M., Klein, D.E., Lee, A., Falasca, M., Isakoff, S.J., Skolnik, E.Y., and Lemmon, M.A. (1998). Specificity and promiscuity in phosphoinositide binding by pleckstrin homology domains. *J. Biol. Chem.* **273**, 30497–30508.
- Knight, Z.A., Feldman, M.E., Balla, A., Balla, T., and Shokat, K.M. (2007). A membrane capture assay for lipid kinase activity. *Nat. Protoc.* **2**, 2459–2466.
- Kono, N., Ohto, U., Hiramatsu, T., Urabe, M., Uchida, Y., Satow, Y., and Arai, H. (2013). Impaired α -TTP-PIPs interaction underlies familial vitamin E deficiency. *Science* **340**, 1106–1110.
- Krylova, I.N., Sablin, E.P., Moore, J., Xu, R.X., Waitt, G.M., MacKay, J.A., Juzumiene, D., Bynum, J.M., Madauss, K., Montana, V., et al. (2005). Structural analyses reveal phosphatidylinositols as ligands for the NR5 orphan receptors SF-1 and LRH-1. *Cell* **120**, 343–355.
- Kumar, D., Gokhale, P., Broustas, C., Chakravarty, D., Ahmad, I., and Kasid, U. (2004). Expression of SCC-S2, an antiapoptotic molecule, correlates with enhanced proliferation and tumorigenicity of MDA-MB 435 cells. *Oncogene* **23**, 612–616.
- Kwiatkowska, K., and Sobota, A. (1999). Signaling pathways in phagocytosis. *BioEssays* **21**, 422–431.
- Lee, A., and Lemmon, M.A. (2001). Analysis of phosphoinositide binding by pleckstrin homology domain from dynamin. *Methods Enzymol.* **329**, 457–468.
- Lev, S. (2010). Non-vesicular lipid transport by lipid-transfer proteins and beyond. *Nat. Rev. Mol. Cell Biol.* **11**, 739–750.
- McLaughlin, S., Wang, J., Gambhir, A., and Murray, D. (2002). PIP(2) and proteins: interactions, organization, and information flow. *Annu. Rev. Biophys. Biomol. Struct.* **31**, 151–175.
- Nile, A.H., Bankaitis, V.A., and Grabon, A. (2010). Mammalian diseases of phosphatidylinositol transfer proteins and their homologs. *Clin. Lipidol.* **5**, 867–897.
- Prinz, W.A. (2010). Lipid trafficking sans vesicles: where, why, how? *Cell* **143**, 870–874.
- Prinz, W.A. (2014). The lipid trade. *Nat. Rev. Mol. Cell Biol.* **15**, 79.
- Sablin, E.P., Krylova, I.N., Fletterick, R.J., and Ingraham, H.A. (2003). Structural basis for ligand-independent activation of the orphan nuclear receptor LRH-1. *Mol. Cell* **11**, 1575–1585.
- Schaaf, G., Ortlund, E.A., Tyeryar, K.R., Mousley, C.J., Ile, K.E., Garrett, T.A., Ren, J., Woolls, M.J., Raetz, C.R., Redinbo, M.R., and Bankaitis, V.A. (2008). Functional anatomy of phospholipid binding and regulation of phosphoinositide homeostasis by proteins of the sec14 superfamily. *Mol. Cell* **29**, 191–206.
- Seibel, N.M., Eljouni, J., Nalaskowski, M.M., and Hampe, W. (2007). Nuclear localization of enhanced green fluorescent protein homomultimers. *Anal. Biochem.* **368**, 95–99.
- Sun, H., Gong, S., Carmody, R.J., Hilliard, A., Li, L., Sun, J., Kong, L., Xu, L., Hilliard, B., Hu, S., et al. (2008). TIPE2, a negative regulator of innate and adaptive immunity that maintains immune homeostasis. *Cell* **133**, 415–426.
- Vivanco, I., and Sawyers, C.L. (2002). The phosphatidylinositol 3-Kinase AKT pathway in human cancer. *Nat. Rev. Cancer* **2**, 489–501.
- Volpicelli-Daley, L.A., Lucast, L., Gong, L.W., Liu, L., Sasaki, J., Sasaki, T., Abrams, C.S., Kanaho, Y., and De Camilli, P. (2010). Phosphatidylinositol-4-phosphate 5-kinases and phosphatidylinositol 4,5-bisphosphate synthesis in the brain. *J. Biol. Chem.* **285**, 28708–28714.
- Wang, Y., Chen, X., Lian, L., Tang, T., Stalker, T.J., Sasaki, T., Kanaho, Y., Brass, L.F., Choi, J.K., Hartwig, J.H., and Abrams, C.S. (2008). Loss of PIP5K β demonstrates that PIP5K isoform-specific PIP₂ synthesis is required for IP₃ formation. *Proc. Natl. Acad. Sci. USA* **105**, 14064–14069.
- Wang, Z., Fayngerts, S., Wang, P., Sun, H., Johnson, D.S., Ruan, Q., Guo, W., and Chen, Y.H. (2012). TIPE2 protein serves as a negative regulator of phagocytosis and oxidative burst during infection. *Proc. Natl. Acad. Sci. USA* **109**, 15413–15418.
- Yuan, T.L., and Cantley, L.C. (2008). PI3K pathway alterations in cancer: variations on a theme. *Oncogene* **27**, 5497–5510.
- Zhang, X., Wang, J., Fan, C., Li, H., Sun, H., Gong, S., Chen, Y.H., and Shi, Y. (2009). Crystal structure of TIPE2 provides insights into immune homeostasis. *Nat. Struct. Mol. Biol.* **16**, 89–90.
- Zhang, Y., Wang, M.Y., He, J., Wang, J.C., Yang, Y.J., Jin, L., Chen, Z.Y., Ma, X.J., Sun, M.H., Xia, K.Q., et al. (2012). Tumor necrosis factor- α induced protein 8 polymorphism and risk of non-Hodgkin's lymphoma in a Chinese population: a case-control study. *PLoS ONE* **7**, e37846.